LETTERS

Earthquakes triggered by silent slip events on Kīlauea volcano, Hawaii

Paul Segall[1], Emily K. Desmarais[1], David Shelly[1], Asta Miklius[2] & Peter Cervelli[3]

Slow-slip events, or 'silent earthquakes', have recently been discovered in a number of subduction zones including the Nankai trough[1–3] in Japan, Cascadia[4,5], and Guerrero[6] in Mexico, but the depths of these events have been difficult to determine from surface deformation measurements. Although it is assumed that these silent earthquakes are located along the plate megathrust, this has not been proved. Slow slip in some subduction zones is associated with non-volcanic tremor[7,8], but tremor is difficult to locate and may be distributed over a broad depth range[9]. Except for some events on the San Andreas fault[10], slow-slip events have not yet been associated with high-frequency earthquakes, which are easily located. Here we report on swarms of high-frequency earthquakes that accompany otherwise silent slips on Kīlauea volcano, Hawaii. For the most energetic event, in January 2005, the slow slip began before the increase in seismicity. The temporal evolution of earthquakes is well explained by increased stressing caused by slow slip, implying that the earthquakes are triggered. The earthquakes, located at depths of 7–8 km, constrain the slow slip to be at comparable depths, because they must fall in zones of positive Coulomb stress change. Triggered earthquakes accompanying slow-slip events elsewhere might go undetected if background seismicity rates are low. Detection of such events would help constrain the depth of slow slip, and could lead to a method for quantifying the increased hazard during slow-slip events, because triggered events have the potential to grow into destructive earthquakes.

A silent earthquake beneath the south flank of Kīlauea volcano on 10–11 November 2000 displaced Global Positioning System (GPS) stations as much as 1.5 cm over about 36 hours[11]. The depth of the subhorizontal fault was not well constrained, but inversions favoured depths of 4–5 km, considerably shallower than the decollement thought to occur at the base of the volcano. We now recognize similar events on 20–21 September 1998, 3–4 July 2003, and 26–27 January 2005 (ref. 12 and additional events have been reported[13]). All four events have similar durations and displacement patterns (Figs 1 and 2). Inversions assuming uniform slip dislocations place the four sources in virtually the same location (Fig. 1). Whereas the November 2000 slow slip was preceded by extreme rainfall[11], the other events were not.

All four slow-slip events were associated with heightened levels of microseismicity (Fig. 2). The cumulative magnitude of the microearthquakes is far too small to explain the observed displacements. For example, the cumulative moment of the 2005 earthquake swarm is $\sim 1.8 \times 10^{14}$ N m, far less than that of the slow slip, 6.8×10^{17} N m. The microearthquakes, concentrated adjacent to the landward edge of the dislocation (Fig. 1), are thus not the source of the deformation.

The association of high-frequency earthquakes with slow slip could be explained by either (1) the earthquakes unpinning the fault, allowing slow slip to occur, or (2) the slow slip stressing the adjacent fault, thereby increasing the seismicity rate. To constrain the onset and duration of fault slip relative to the microearthquakes, we invert the GPS observables during the 2005 slow event directly for fault slip as a function of time[11]. The slow slip started early on 26 January 2005, well before the dramatic increase in seismicity, and

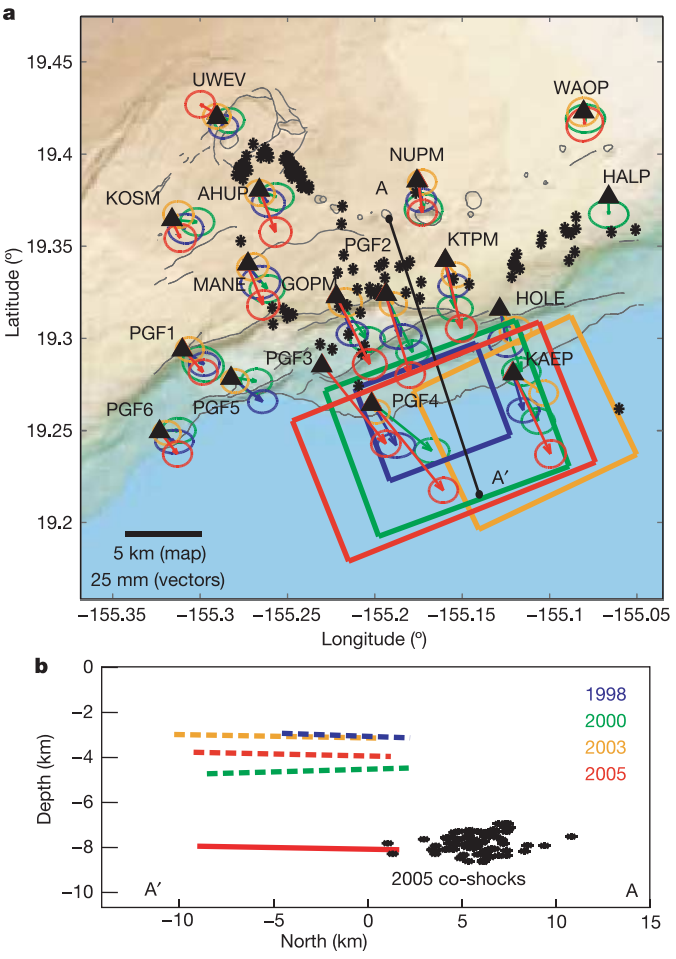

Figure 1 | Displacements and inferred slip zones for four silent slip events. a, Map view. Vectors indicate displacements determined as the difference between the mean position before and after the event. Ellipses represent 95% confidence intervals. Rectangles show surface projections of best-fitting dislocations found by non-linear optimization, using a simulated annealing procedure[27]. Asterisks indicate relocated earthquakes accompanying the 2005 slip event. **b**, Cross-section. Dashed lines represent dislocations from inversion of GPS-derived displacements. The solid red line indicates the 2005 event with depth constrained by seismicity (see text). GPS station locations (triangles) indicated with abbreviations.

[1]Geophysics Department, Stanford University, Stanford, California 94305, USA. [2]USGS Hawaii Volcano Observatory, PO Box 51 Hawaii National Park, Hawaii 96718-0051, USA. [3]USGS Alaska Volcano Observatory, 4200 University Drive, Anchorage, Alaska 99508, USA.

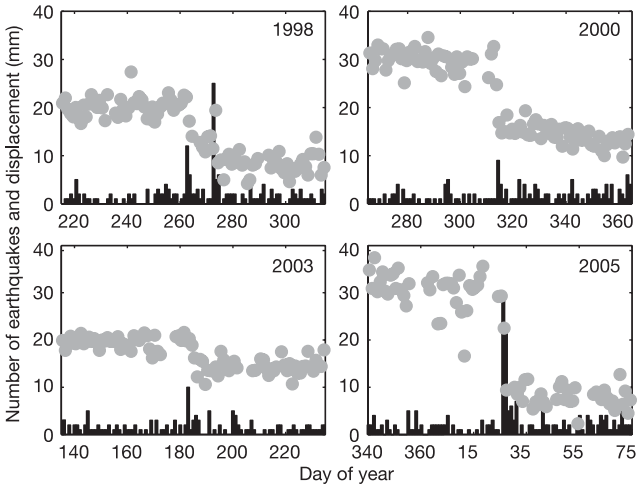

Figure 2 | Temporal association of deformation and seismicity. North component of displacement of GPS station KAEP (grey circles) and number of Kīlauea south-flank earthquakes per day (black histogram). Note that the seismicity rate increases during periods of rapid displacement.

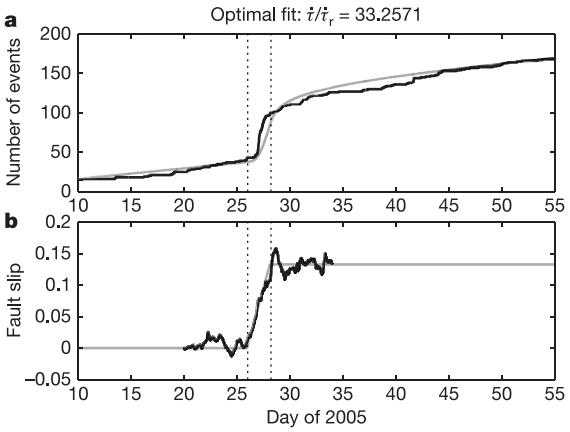

Figure 3 | Cumulative number of earthquakes compared to that predicted for a slip event by equation (3). a, Observed earthquake count in hourly bins (black line); predicted for the slow-slip event (grey line). Vertical dotted lines mark the beginning and end of the slow-slip event. **b**, Inverted slip history estimated directly from the GPS phase data (black line), using a Kalman filter procedure[11]. Fault slip is allowed to vary as a random walk in time, with scale parameter $\sigma_s = 0.015\,\mathrm{mm\,yr^{-1/2}}$. The ramp function illustrates the stress history used to derive the predicted seismicity rate (grey line).

continued for approximately two days (Fig. 3), supporting the second interpretation. The triggered earthquakes should thus properly be thought of as 'co-shocks' and aftershocks of the otherwise silent earthquakes.

Dieterich's seismicity rate theory[14] is used to quantitatively relate the slip and seismicity. The seismicity rate R is related to the background seismicity rate r and a state variable γ, as:

$$R = \frac{\mathrm{d}N}{\mathrm{d}t} = \frac{r}{\gamma \dot{\tau}_r} \tag{1}$$

where N is the number of events, and $\dot{\tau}_r$ is the background stressing rate. The seismicity state variable evolves according to:

$$\mathrm{d}\gamma = \frac{1}{a\sigma}[\mathrm{d}t - \gamma \mathrm{d}\tau + \gamma(\tau/\sigma - \alpha)\mathrm{d}\sigma] \tag{2}$$

where a and α are constitutive constants, and τ and σ are the shear and effective normal stresses, respectively. Because normal stress variations may be largely balanced by undrained changes in pore pressure, we assume $\mathrm{d}\sigma = 0$; in fact the stress variations are understood to be changes in the Coulomb stress. Dieterich[14] showed that the seismicity rate following a step change in shear stress $\Delta\tau$, followed by a return to the background stressing rate $\dot{\tau}_r$, yields the modified Omori law with aftershock duration given by $t_a = a\sigma/\dot{\tau}_r$.

To model the triggered seismicity, we approximate the slip history with a ramp function (Fig. 3b). Before the onset of accelerated slip, $t < t_0$, the background stressing rate is $\dot{\tau}_r$. During the event $t_0 < t < t_1$ the stressing rate increases to $\dot{\tau}$; for $t > t_1$ the stressing rate returns to background. For this stress history the predicted seismicity rate is found from equations (1) and (2) (see Methods). To compare with observations we compute the cumulative number of earthquakes, $N(t)$, determined by integrating $R(t)$:

$$N(t) = \begin{cases} rt_a \ln\left[\frac{\dot{\tau}_r}{\dot{\tau}}\left(\exp\left(\frac{\dot{\tau}(t-t_0)}{a\sigma}\right) - 1\right) + 1\right] & \text{for } t_0 < t < t_1 \\ rt_a \ln\left[\frac{\exp\left(\frac{t-t_1}{t_a}\right)+C}{1+C}\right] & \text{for } t > t_1 \end{cases} \tag{3}$$

where

$$C = \left[\left(1 - \frac{\dot{\tau}_r}{\dot{\tau}}\right)\exp\left(-\frac{\dot{\tau}(t_1 - t_0)}{a\sigma}\right) + \frac{\dot{\tau}_r}{\dot{\tau}} - 1\right] \tag{4}$$

$N(t)$ depends on five parameters: (1) the background rate r, (2) the aftershock decay time, t_a; (3) the ratio of the event to the background stressing rate, $\dot{\tau}/\dot{\tau}_r$, (4) the onset t_0 and (5) the duration $t_1 - t_0$ of the slip event. Note that $\dot{\tau}/a\sigma = \dot{\tau}/\dot{\tau}_r t_a$.

The background rate r of ~1.33 events per day is estimated from the Hawaii Volcano Observatory (HVO) catalogue before and well after the slow-slip event. The onset time (GMT midnight on 26 January) and duration (2.2 days) of the slow event are determined from the GPS data (Fig. 3b). A t_a of 10 to 20 days is found from the decay of aftershocks following the 30 June 1997, magnitude $M_w = 5.5$ south-flank earthquake. The only parameter not determined *a priori* is the ratio of stressing rates $\dot{\tau}/\dot{\tau}_r$.

We fitted the cumulative number of earthquakes to equation (3) with $t_a = 10$. The best fit, obtained for an increase in stressing rate of a factor of 33, provides satisfactory agreement with the earthquake data (Fig. 3), especially considering the single adjustable parameter. A better fit is obtained by reducing t_a to seven days. Whether this indicates temporal or spatial variation in t_a (the 1997 earthquake was roughly 20 km from the swarm earthquakes) is unknown.

The spatial association of the silent slip and its co-shocks is clear when viewed on a map, but the depth of the slow-slip event is difficult to constrain solely on the basis of the GPS observations. Although the catalogue earthquake depths are scattered over a broad range, relocations of south-flank earthquakes illuminate a sub-horizontal plane[15,16]. Hansen *et al.*[17] used a temporary deployment of 29 three-component seismometers along with the HVO permanent network jointly to locate earthquakes and determine the three-dimensional seismic velocity structure. They found that earthquakes occurring on the central south flank from November 1999 to June 2000 lie on a nearly horizontal surface at a depth of 7 to 9 km.

The Hansen *et al.*[17] hypocentres can be used to improve the locations of the swarm events accompanying slow slips. We focus on the most energetic January 2005 swarm. From their catalogue locations, we infer that quakes during the other slow events are located at comparable depths. A 'double difference' relocation[18] of the January 2005 swarm events relative to the 1999–2000 events (see Methods) demonstrates that the swarm events were located at the same depth as the background seismicity, 7 to 9 km (Fig. 1).

The depth of the swarm earthquakes, and the likelihood that they were triggered by the slow slip, constrains the depth of the slow slip. Specifically, slow slip must have occurred at depths for which the induced stresses favour slip in the swarm. If the slow slip is too shallow the earthquakes locate in a stress shadow and are thus inconsistent with triggering. Varying the depth of the best-fitting dislocation maps the depth range consistent with the triggered

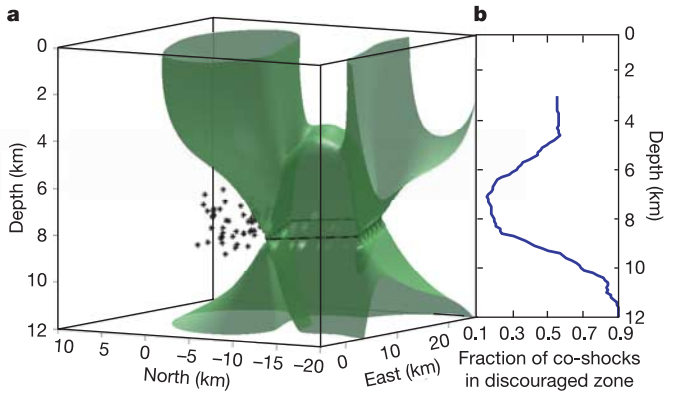

Figure 4 | Earthquake locations in relation to Coulomb stress change due to fault slip. a, January 2005 earthquakes (asterisks) and isosurface of constant Coulomb stress change (CSC) on horizontal planes, with dislocation at 8 km depth as indicated by dashed slice. Outside the green surface the stress change encourages slip. For a dislocation surface at 4–5 km depth, a majority of the earthquakes fall within the zone of negative CSC. **b**, Fraction of earthquakes for which CSC < 0 as a function of the depth of the slow-slip event. The minimum at a depth of 6.5 to 8.5 indicates the preferred depth of the slow-slip zone.

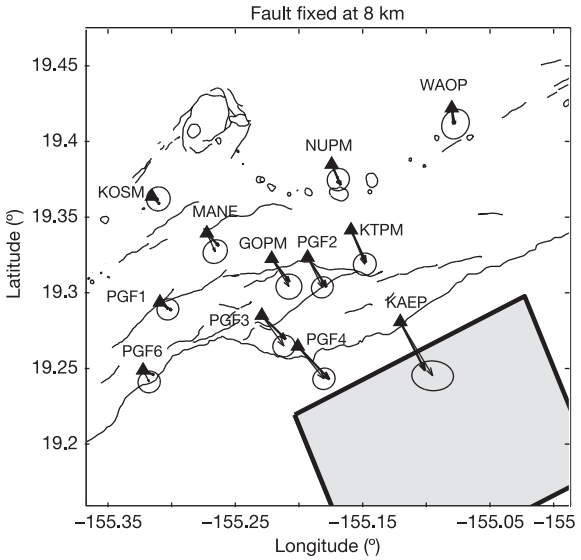

Figure 5 | Dislocation at a depth of 8 km fits the GPS data well. Observed (thin vectors with 95% confidence ellipses) and predicted (bold vectors) displacements during the January 2005 silent slip event with dislocation constrained to depth of 8.0 km. Surface projection of best fitting dislocation shown as rectangle.

earthquakes (Fig. 4). The best fit occurs when the slip event is at the same depth as the earthquakes, 6.5–8.5 km. At this depth the shear stress concentration at the edge of the dislocation is focused on the earthquake swarm. The silent slip event and its co-shocks are thus probably coplanar and located at a depth of 6.5–8.5 km.

Is the depth of the silent slip event inferred from the earthquakes consistent with the geodetic observations? The best-fitting dislocation constrained to a depth of 8.0 km (Fig. 5) is in fact consistent with the data at the few-millimetre level. Depth-varying elastic properties and non-planar topography favour deeper sources relative to uniform half-space models, although the effect is relatively minor.

Kīlauea suffered an $M_w = 7.7$ earthquake and tsunami in 1975 (ref. 19). Despite the fact that both geodetic data[20] and the tsunami source[21] require slip offshore, the aftershocks were restricted to a narrow strip between the rift zones and the coastline. Indeed, south-flank earthquakes rarely occur offshore, despite the fact that the geodetic data require extensive slip there[22,23]. These observations indicate a transition from stick-slip behaviour between the rift zone and the coast to stable sliding offshore. Slow-slip events seem to occur in the transition between these two domains. Modelling studies indicate that transient slip events occur in transitions from velocity weakening to velocity strengthening friction[24], or where velocity-weakening patches in an otherwise creeping fault are near the critical nucleation dimension[25]. On Kīlauea the transition in frictional behaviour might result from temperature and pressure variations with distance from the rift zone[26].

Our results have implications for silent slip events in subduction zones. (A slow earthquake on the San Andreas fault[10] appears to have been triggered in part by a sequence of $M_w = 3+$ earthquakes, which initiated two hours before detectable strain changes, and is thus very different from the Kīlauea slow events.) Microseismicity rates on Kīlauea are much higher than in some subduction zones. A rate increase of a factor of 35 is dramatic on Kīlauea, but might go unnoticed in subduction zones with few earthquakes located on the plate interface. Given our findings, a concerted effort should be made to search for very small earthquakes accompanying slow-slip events elsewhere.

Slow-slip events in subduction zones appear to be located down-dip of the locked zone, so that transient slip acts to stress the seismogenic fault. If small events are triggered, as we observe on Kīlauea, then the potential exists for one of these to grow into a destructive earthquake. A $M_w = 6.7$ thrust earthquake coincided with the end of the 2002 slow-slip event in Guerrero, Mexico[24]. It is possible to quantify the increased hazard associated with slow-slip events by the increase in seismicity rate, which depends on the duration of the slow slip relative to t_a and the increase in stressing rate $\dot{\tau}/\dot{\tau}_r$. The peak seismicity rate $1/(C+1)$ occurs at the end of the slow-slip event t_1 (see Methods). Of course, the nucleation of an earthquake does not determine its ultimate size. The longer the plate boundary remains locked, however, the higher the ambient stresses become, and the more likely it is that a triggered event will grow into a major earthquake. It is possible that as the stress increases the size of co-shocks triggered during slow events will increase, making them more easily detected.

METHODS

Predicted seismicity rate. At $t = 0$, γ takes the value $1/\dot{\tau}_r$. Ignoring changes in effective normal stress, for $0 < t < t_1$ the stressing rate is constant at $\dot{\tau}$, so that equation (2) reduces to:

$$\frac{d\gamma}{dt} = \frac{1}{a\sigma}[1 - \gamma\dot{\tau}] \tag{5}$$

which has solution:

$$\gamma = \left(\frac{1}{\dot{\tau}_r} - \frac{1}{\dot{\tau}}\right)\exp\left(-\frac{\dot{\tau}t}{a\sigma}\right) + \frac{1}{\dot{\tau}} \quad \text{for} \quad 0 < t < t_1 \tag{6}$$

given the initial condition $\gamma(t = 0) = 1/\dot{\tau}_r$. For $t > t_1$ the stressing rate is again constant, but at the background rate. The solution to equation (5) is thus of a similar form to equation (6), but the initial condition is now given by $\gamma_1 \equiv \gamma(t_1)$, that is, equation (6) evaluated at t_1. The result is:

$$\gamma = \left(\gamma_1 - \frac{1}{\dot{\tau}_r}\right)\exp\left(-\frac{\dot{\tau}_r(t - t_1)}{a\sigma}\right) + \frac{1}{\dot{\tau}_r} \quad \text{for} \quad t > t_1 \tag{7}$$

The seismicity rate can now be calculated simply from equation (1).

$$\frac{R(t)}{r} = \begin{cases} \left[\left(1 - \frac{\dot{\tau}_r}{\dot{\tau}}\right)\exp\left(-\frac{\dot{\tau}(t - t_0)}{a\sigma}\right) + \frac{\dot{\tau}_r}{\dot{\tau}}\right]^{-1} & t_0 < t < t_1 \\ \left\{C\exp\left(-\frac{(t - t_1)}{t_a}\right) + 1\right\}^{-1} & t > t_1 \end{cases} \tag{8}$$

We note that if the duration of the slip event is long compared to $a\sigma/\dot{\tau}$ the seismicity rate approaches a steady state that is a factor of $\dot{\tau}/\dot{\tau}_r$ over the background rate. Following the event, as $t \to \infty$, the seismicity rate returns to background. We also note that as $\dot{\tau} \to \infty$ and $(t_1 - t_0) \to 0$ such that the product $\dot{\tau}(t_1 - t_0) \to \Delta\tau$, equation (8) reduces to equation (12) in ref. 14, which gives the Omori-like decay of events following a step change in stress.

To estimate the aftershock duration t_a we fitted the cumulative number of earthquakes following a high-frequency mainshock. Dieterich[14] found that the number of earthquakes following a step change in shear stress $\Delta\tau$ is given by:

$$N(t) = rt_a \ln\{e^{\Delta\tau/a\sigma}(e^{t/t_a} - 1) + 1\} \quad (9)$$

Relative earthquake locations. The data are arrival times for the 2005 events, determined by the Hawaiian Volcano Observatory, and arrival times for the 1999–2000 events, provided by the University of Wisconsin. We used a one-dimensional layered velocity model that approximates the three-dimensional model of ref. 17. The 1999–2000 events were fixed at the locations determined by Hansen *et al.*[17]. To minimize potential bias from the one-dimensional model, we weighted the differential times between the 1999/2000 and 2005 events three times more heavily than the remaining differential times.

Received 11 January; accepted 23 May 2006.

1. Hirose, H., Hirahara, K., Kimata, F., Fujii, N. & Miyazaki, S. A slow thrust slip event following the two 1996 Hyuganada earthquakes beneath the Bungo Channel, southwest Japan. *Geophys. Res. Lett.* **26,** 3237–3240 (1999).
2. Ozawa, S. *et al.* Detection and monitoring of ongoing aseismic slip in the Tokai region, central Japan. *Science* **298,** 1009–1012 (2002).
3. Miyazaki, S., McGuire, J. & Segall, P. A transient subduction zone slip episode in southwest Japan observed by the nationwide GPS array. *J. Geophys. Res.* **108,** 2087–2087 (2003).
4. Dragert, H., Wang, K. L. & James, T. S. A silent slip event on the deeper Cascadia subduction interface. *Science* **292,** 1525–1528 (2001).
5. Miller, M. M., Melbourne, T., Johnson, D. J. & Sumner, W. Q. Periodic slow earthquakes from the Cascadia subduction zone. *Science* **295,** 2423–2423 (2002).
6. Kostoglodov, V. *et al.* A large silent earthquake in the Guerrero seismic gap, Mexico. *Geophys. Res. Lett.* **30,** 1807–1810 (2003).
7. Rogers, G. & Dragert, H. Episodic tremor and slip on the Cascadia subduction zone: The chatter of silent slip. *Science* **300,** 1942–1943 (2003).
8. Obara, K., Hirose, H., Yamamizu, F. & Kasahara, K. Episodic slow slip events accompanied by non-volcanic tremors in southwest Japan subduction zone. *Geophys. Res. Lett.* **31,** L23602, doi:10.1029/2004GL020848 (2004).
9. Kao, H. *et al.* A wide depth distribution of seismic tremors along the northern Cascadia margin. *Nature* **436,** 841–844 (2005).
10. Linde, A., Gladwin, M., Johnston, M., Gwyther, R. & Bilham, R. A slow earthquake sequence on the San Andreas fault. *Nature* **383,** 65–68 (1996).
11. Cervelli, P., Segall, P., Johnson, K., Lisowski, M. & Miklius, A. Sudden aseismic fault slip on the south flank of Kilauea volcano. *Nature* **415,** 1014–1018 (2002).
12. Segall, P., Desmarais, E., Miklius, A. & Okubo, P. (Nearly) silent earthquakes on volcanoes. *Trans. AGU Fall Meet. Suppl.* **86**(52), G43A-01 (2005).
13. Brooks, B., Foster, J., Bevis, M., Frazer, L. & Behn, M. Slow earthquakes on the flank of Kilauea volcano, Hawaii. *Trans. AGU Fall Meet. Suppl.* **86**(52), G53B-0879 (2005) .
14. Dieterich, J. A constitutive law for rate of earthquake production and its application to earthquake clustering. *J. Geophys. Res.* **99,** 2601–2618 (1994).
15. Got, J., Frechet, J. & Klein, F. Deep fault plane geometry inferred from multiplet relative relocation beneath the south flank of Kilauea. *J. Geophys. Res.* **99,** 15375–15386 (1994).
16. Got, J.-L. & Okubo, P. New insights into Kilauea's volcano dynamics brought by large scale relative relocation of microearthquakes. *J. Geophys. Res.* **108,** 2337–2350 (2003).
17. Hansen, S., Thurber, C., Mandernach, M., Haslinger, F. & Doran, C. Seismic velocity and attenuation structure of the East Rift Zone and south flank of Kilauea volcano, Hawaii. *Bull. Seismol. Soc. Am.* **94,** 1430–1440 (2004).
18. Waldhauser, F. & Ellsworth, W. L. A double-difference earthquake location algorithm: method and application to the Northern Hayward Fault, California. *Bull. Seismol. Soc. Am.* **90,** 1353–1368 (2000).
19. Nettles, M. & Ekstrom, G. Long-period source characteristics of the 1975 Kalapana, Hawaii, earthquake. *Bull. Seismol. Soc. Am.* **94,** 422–429 (2004).
20. Owen, S. & Burgmann, R. An increment of volcano collapse: Kinematics of the 1975 Kalapana, Hawaii, earthquake. *J. Volcan. Geotherm. Res.* **150,** 163–185 (2006).
21. Ma, K.-F., Kanamori, H. & Satake, K. Mechanism of the 1975 Kalapana, Hawaii, earthquake inferred from tsunami data. *J. Geophys. Res.* **104,** 13153–13168 (1999).
22. Delaney, P. *et al.* Volcanic spreading at Kilauea, 1976–1996. *J. Geophys. Res.* **103,** 18003–18023 (1998).
23. Owen, S. *et al.* Rapid deformation of Kilauea volcano: Global positioning system measurements between 1990 and 1996. *J. Geophys. Res.* **105,** 18983–18998 (2000).
24. Liu, Y. & Rice, J. R. Aseismic slip transients emerge spontaneously in 3d rate and state modeling of subduction earthquake sequences. *J. Geophys. Res.* **110,** B08307, doi:10.1029/2004JB003424 (2005).
25. Kato, N. Interaction of slip on asperities: Numerical simulation of seismic cycles on a two-dimensional planar fault with nonuniform frictional property. *J. Geophys. Res.* **109,** B12306, doi:10.1029/2004JB003001 (2004).
26. Segall, P., Cervelli, P. & Miklius, A. Insights from deformation during the Pu'u O'o eruption of Kilauea volcano. *Eos Trans. AGU Fall Meet. Suppl.* **83**(47), abstr. V62C-02 (2002).
27. Cervelli, P., Murray, M., Segall, P., Aoki, Y. & Kato, T. Estimating source parameters from deformation data, with an application to the March 1997 earthquake swarm off the Izu Peninsula, Japan. *J. Geophys. Res.* **106,** 11217–11238 (2001).

Acknowledgements We gratefully acknowledge C. Thurber for providing seismic data from the University of Wisconsin 1999/2000 experiment, P. Okubo for help with HVO seismic data, the University of Hawaii for exchange of GPS data, and D. Swanson for editorial comments.

Author Contributions P.S. and E.K.D. jointly modelled GPS and seismic data. P.S. derived the seismicity rate results. D.S. relocated the earthquakes. A.M. processed GPS data and first detected the events studied. P.C. helped with time-dependent slip inversion. All authors discussed results and commented on manuscript.

Author Information Reprints and permissions information is available at npg.nature.com/reprintsandpermissions. The authors declare no competing financial interests. Correspondence and requests for materials should be addressed to P.S. (segall@stanford.edu).